Rheologica Acta (2021) 60:803–817
https://doi.org/10.1007/s00397-021-01304-1

ORIGINAL CONTRIBUTION

Elongational viscosity and brittle fracture of bidisperse blends of a high and several low molar mass polystyrenes

Manfred H. Wagner[1] · **Esmaeil Narimissa**[2,3] · **Taisir Shahid**[4,5]

Received: 14 May 2021 / Revised: 18 August 2021 / Accepted: 19 September 2021 / Published online: 22 October 2021

Abstract

Elongational viscosity data of four well-characterized blends consisting of 10% mass fraction of monodisperse polystyrene PS-820k (molar mass of 820 kg/mol) and 90% matrix polystyrenes with a molar mass of 8.8, 23, 34, and 73 kg/mol, respectively, as reported by Shahid et al. Macromolecules 52: 2521–2530, 2019 are analyzed by the extended interchain pressure (EIP) model including the effects of finite chain extensibility and filament rupture. Except for the linear-viscoelastic contribution of the matrix, the elongational viscosity of the blends is mainly determined by the high molar mass component PS-820k at elongation rates when no stretching of the lower molar mass matrix chains is expected. The stretching of the long chains is shown to be widely independent of the molar mass of the matrix reaching from non-entangled oligomeric styrene (8.8 kg/mol) to well-entangled polystyrene (73kg/mol). Quantitative agreement between data and model can be obtained when taking the interaction of the long chains of PS-820k with the shorter matrix chains of PS-23k, PS-34k, and PS-73k into account. The interaction of long and short chains leads to additional entanglements along the long chains of PS-820k, which slow down relaxation of the long chains, as clearly seen in the linear-viscoelastic behavior. According to the EIP model, an increased number of entanglements also lead to enhanced interchain pressure, which limits maximal stretch. The reduced maximal stretch of the long chains due to entanglements of long chains with shorter matrix chains is quantified by introducing an effective polymer fraction of the long chains, which increases with the increasing length of the matrix chains resulting in the excellent agreement of experimental data and model predictions.

Keywords Polymer melt · Polymer blend · Fracture · Chain scission · Elongation · EIP model · Interchain pressure · Finite extensibility

Introduction

While there seems to be general agreement on the universality of the linear-viscoelastic behavior of well-entangled monodisperse linear polymer melts and solutions based on only three material parameters (plateau modulus, characteristic time, and the number of entanglements), this universality is lost in the nonlinear viscoelastic regime as especially apparent in elongational flows (Huang et al. 2013a, b, 2015). Polymer melts exhibit a monotonic strain-rate thinning behavior of the elongational viscosity, while polymer solutions with the same number of entanglements exhibit an initial strain-rate thinning behavior followed by a strong increase of the elongational viscosity, which occurs at rates comparable to the reciprocal Rouse time of the chains. This nonuniversality is now well established experimentally; however, its molecular origin and in particular the absence of extension thickening in the case of polymer melts has

✉ Manfred H. Wagner
manfred.wagner@tu-berlin.de

Esmaeil Narimissa
esmaeiln@technion.ac.il

[1] Polymer Engineering/Polymer Physics, Berlin Institute of Technology (TU Berlin), Ernst-Reuter-Platz 1, 10587 Berlin, Germany

[2] Dept. of Chemical Engineering, Technion–Israel Institute of Technology (IIT), Technion City, 32 000 Haifa, Israel

[3] Dept. of Chemical Engineering, Guangdong Technion–Israel Institute of Technology (GTIIT), Shantou 515063, China

[4] Bio and Soft Matter, Institute on Condensed Matter and Nanoscience, Université Catholique de Louvain, Ottignies-Louvain-la-Neuve, Belgium

[5] DSM Materials Science Center, P.O. Box 18, NL-6160 MD, Geleen, The Netherlands

sparked different theoretical explanations as discussed, e.g., by Narimissa et al. (2020a, 2021) and Ianniruberto et al. (2020).

Marrucci and Ianniruberto (2004) proposed that flow-induced contraction of the tube diameter from its equilibrium value results in an "interchain pressure" relaxation effect. By incorporating this concept in the molecular stress function (MSF) theory, Wagner et al. (2005) and Wagner and Rolón-Garrido (2009a, b) were able to obtain quantitative agreement for monodisperse polystyrene (PS) melts. They assumed that chain stretch is balanced by two restoring tensions with weights of 1/3 in the longitudinal direction of the tube, due to a linear entropic spring force, and 2/3 in the lateral direction, due to a nonlinear interchain tube pressure, both of which are characterized by the Rouse stretch relaxation time. This approach is in quantitative agreement with the time-dependent and steady-state elongational viscosity of monodisperse polystyrene melts investigated by Bach et al. (2003). In bidisperse polymer blends consisting of a long and a short-chain component as investigated by Nielsen et al. (2008), the interchain pressure is reduced in accordance with dynamic dilation of the tube. Implementation of the dilation effect into the evolution equation of the stretch led to a quantitative description of the elongational behavior of bidisperse polystyrene blends (Wagner 2011). Later, this extended interchain pressure (EIP) model was successfully used in modeling entangled polystyrene solutions (Wagner 2014, 2015; Wagner et al. 2015; Narimissa et al. 2020a, 2020b) and melts of other polymers than polystyrene (Narimissa et al. 2021).

Alternatively, Yaoita et al. (2012) and Ianniruberto et al. (2012) proposed that the monotonic thinning behavior observed in the melt state is due to an alignment-induced reduction of the monomeric friction under fast elongational flow. According to this hypothesis, stretching of the chains in fast flows induces strong local anisotropy and results in a decrease of the (monomeric) friction coefficient of the chains. This should mainly affect entangled polymer melts since in solution the small molecules do not align. However, recent work by Huang et al. (2013b) suggested that in solutions of polystyrene in oligomeric styrene, friction reduction may also take place via nematic interactions between the oligomers and the polymer molecules, and the importance of this process was suggested to increase with the size of the oligomers, i.e., longer oligomeric chains would increase friction reduction and thereby decrease the elongational viscosity. Subsequently, an empirical nematic interaction parameter was included in the nonlinear tube model, defined as the ratio of the order parameter of the short molecules to the average order parameter of the system. The resulting model allowed obtaining a more accurate description of the properties of various polystyrene melts and solutions (Ianniruberto et al. 2020).

From the above, it is evident that the role of solvent molar mass on the reduction of extension hardening when going from polystyrene solutions in oligomeric styrene to polystyrene melts, is of prime interest in developing molecular constitutive equations for polymer melts and solutions and in advancing polymer physics. While Nielsen et al. (2008) investigated bidisperse polymer blends consisting of 4 and 14% of a long-chain component with a molar mass of 390 kg/mol in a matrix of a short-chain component with a molar mass of either 50 or 100 kg/mol, Shahid (2018) and Shahid et al. (2019) explored systematically the transition from polymer solutions to polymer melts in uniaxial extension by means of diluting 10% of long polystyrene chains (PS-820k) in matrices ranging from an unentangled styrene oligomer OS8.8k with a molar mass of 8.8 kg/mol to entangled polymer melts with different molar masses from ranging from 23 to 73 kg/mol. The elongation rates were selected in such a way that friction reduction is solely governed by the suggested long-chain matrix nematic interaction, i.e., the reciprocal Rouse times of the matrices exceed the elongation rates, so that the short chains should not stretch over the entire range of investigated strain rates. Based on their experimental results, the authors concluded that all PS blends have the same apparent steady-state elongational viscosity when compared at the same distance in temperature from the glass transition temperature, and that as long as the matrix exceeds a "critical" molar mass (estimated as 4 kg/mol) the hypothetical nematic interaction of the long chains with the matrix does not exist or is at least constant and independent of the molar mass and entanglement state of the matrix molecules.

These investigations were made possible due to substantial progress in measuring the elongational viscosity of polymer melts and solutions up to high Hencky strains by use of the filament stretching rheometer with locally controlled deformation and deformation rate developed by Hassager and coworkers (Huang et al. 2016a). By measuring the local diameter of the polymer sample during elongation, the true Hencky strain and strain rate can be determined and controlled, while by elongational rheometers prescribing the global deformation of the filament only nominal values of strain and strain rate can be obtained. A further achievement of the filament stretching rheometer as shown by Huang et al. (2016b, Huang and Hassager 2017) and Huang (2019) was that when the true Hencky strain rate is controlled rather than the nominal Hencky rate, the four failure zones of the so-called Malkin plot (Malkin and Petrie 1997) (purely viscous zone, viscoelastic zone with failure by necking, rubbery zone, and glassy zone) are reduced to just two possible states: liquid or solid, and a clear distinction exists between liquid-like behavior (unlimited steady-state elongation) and solid-like behavior (brittle fracture). A quantitative criterion for brittle fracture of entangled polymer

liquids (Wagner et al. 2018) was recently extended by taking finite chain extensibility and polymer fraction of the solutions into account (Wagner et al. 2021a, 2021b). Filament rupture follows from the scission of primary C–C bonds when the strain energy of an entanglement segment reaches the bond-dissociation energy of the covalent bond. Thermal fluctuations lead to a short-time concentration of the strain energy on one C–C bond of the entanglement segment, and the chain ruptures.

In this paper, we present a quantitative analysis of the elongational viscosity data of Shahid et al. (2019) of well-characterized blends consisting of 10% mass fraction of monodisperse polystyrene PS-820k (molar mass of 820 kg/mol) and 90% matrix polystyrenes with a molar mass of 8.8, 23, 34, and 73 kg/mol, respectively. Modeling is based on the extended interchain pressure (EIP) model including the effects of finite chain extensibility, and on the recently developed fracture criterion for brittle fracture of polymer melts and solutions (Wagner et al. 2021a, 2021b).

Experimental data and LVE characterization

The molecular characteristics of the polystyrene samples and the blends prepared are summarized in Table 1 and the data are taken from Shahid (2018) and Shahid et al. (2019). The blends are named in the form of PS-820k/X, where 820k characterizes the molar mass of the high molar mass polystyrene with 10 mass % in the blend, and X the molar mass of the matrix styrene oligomer or polystyrene with 90% in the blend. The number of entanglements of the monodisperse melts was calculated from the ratio of the molar mass M to the entanglement molar mass M_e,

$$Z = \frac{M}{M_e} \tag{1}$$

In the blends, the number of long-chain/long-chain entanglements is given by

$$Z_{LL} = \frac{M_L}{M_e}\phi \tag{2}$$

with M_L being the molar mass of PS-820k and $\phi = 0.1$the polymer fraction of the long chains in the blends. Following Shahid et al. (2019), a value of $M_e = 15$ kg/mol is used here. The number of entanglements of the short chains with long and short chains remains nearly constant at $Z_S = Z$. The Rouse time, which is the longest relaxation time of an unentangled chain, is very important in elongational flow as polymer chains are presumed to be stretched when the flow rate exceeds the reciprocal of this characteristic time. In the tube model (Doi and Edwards 1978, 1979), this relaxation time is given as

$$\tau_R = Z^2\tau_e \tag{3}$$

where τ_e is the relaxation time of a chain segment between entanglements. The value of τ_e depends on the iso-T_g condition and a value of $\tau_e = 0.12$ s at $T_e = T_g + 31.4$ K was used by Shahid et al. (2019) leading to the Rouse times presented in Table 1. They assumed that the short chains start to stretch at a Weissenberg number $Wi = \dot{\varepsilon}\tau_R = 1$, i.e., at elongation rates of 0.35, 1.59, 3.45, and 25 s^{-1} for the matrix polymers of molar mass equal to 73, 34, 23, and 8.8 kg/mol, respectively. Therefore, in order to avoid stretching of the short components, the highest strain rate used was 0.2 s^{-1}. However, we note from our earlier analysis (Wagner et al. 2021b) of polystyrene solution data (André et al. 2021) that stretching starts already at $Wi \cong 1/3$, i.e., at $\dot{\varepsilon} \geq 0.1$ s^{-1} for PS-73k. Also given in Table 1 is the Graessley parameter $Gr = Z_L/Z_S^3$ with $Z_L$being the total number of entanglements of a chain of PS-820k with $Z_L = M_L/M_e$ in the melt state, largely independent of the matrix as long as the matrix chains are long enough to be entangled. At small values of Gr relaxation by reptation along the tube formed by long and short chains dominate, while at large values of the Graessley parameter, terminal relaxation via constraint release by the short chains is the dominant relaxation mechanism for the long chains (Struglinski and Graessley 1985).

Table 1 Characterization of polystyrene samples and blends

Molar mass[kg/mol]	PDI [−]	Z [−]	T_g [°C]	τ_R at Te °C [s]
820	1.02	54.7	106.6	359
73	1.08	5	105.6	2.9
34	1.11	2	103.3	0.63
23	1.09	1	92.4	0.29
8.8	1.10	0	94.6	0.04
Blend	Z_{LL}/Z_S	Gr	T_g [°C]	T_e [°C]
PS-820k/73k	5/5	0.4	106.6	138
PS-820k/34k	5/2	6.8	104.7	136
PS-820k/23k	5/1	55	103.5	135
PS-820k/8.8k	5/0	-	98.6	130

Details of mechanical spectroscopy and elongational viscosity measurements are presented in (Shahid 2018). Elongational measurement using a VADER 1000 (Huang et al. 2016a) were performed at iso-T_g temperatures T_e, i.e., temperatures with equal distance to the glass transition temperature T_g with $T_e = T_g + 31.4$ K. Storage (G') and loss modulus (G'') were measured at several temperatures between 120 and 170 °C, and the resulting mastercurves were shifted to T_e by time-temperature shifting. From the mastercurves of G' and G'' as reported by Shahid (2018), we obtain parsimonious relaxation spectra $G(t)$ with

$$G(t) = \sum_{i=1} g_i \exp\left(-t/\tau_i\right) \tag{4}$$

for characterization of the linear viscoelasticity (LVE) in the experimentally accessible window. The partial moduli g_i and relaxation times τ_i as determined by the IRIS software (Winter and Mours 2006) are presented in Table 2 and result in excellent agreement with the linear-viscoelastic data of G' and G'' as shown in Fig. 1. The mastercurves of G' and G'' of PS-820k/8.8k are compared with those of PS-820k/23k (Fig. 1a), PS-820k/34k (Fig. 1b), and PS-820k/73k (Fig. 1c). The linear viscoelastic data clearly show a fast relaxation of the short matrixes at high frequencies, followed by the relaxation of the long chains at lower frequencies. The long chains in sample PS-820k/8.8k with about 5 entanglements show the indication of a rubbery plateau with two crossovers of G' and G'' at a modulus of about 10^3 Pa. This rubbery plateau gradually diminishes in the blends with longer matrix molecules of PS-23k (Fig. 1a) and PS-34k (Fig. 1b), and it disappears totally in the case of matrix PS-73k (Fig. 1c). Despite the fact that the same concentration of long chains is used for all blends, the terminal relaxation time increases with increasing molar mass of the matrix chains due to the entanglements formed between long and short chains and therefore the slower relaxation of the long chains. With the increasing molar mass of the matrix, a rubbery plateau is emerging at a modulus of about 10^5 Pa, and this signature of entangled chains is moving to lower frequencies with increasing molar mass of the matrix. For PS-820k/73k, the relaxation from the high modulus plateau is totally overshadowing the plateau of the long chains (Fig. 1c). However, the effect of the long chains is still clearly visible in Fig. 2, which shows the loss tangent δ as a function of the absolute value of the complex modulus G^* at $T_e = T_g + 31.4$ K. The minimum at high G^* indicates the plateau modulus of PS melt at about $G_{\mathrm{Nm}} \cong 2.5 \cdot 10^5$ Pa (Wagner et al. 2021b), while the minimum at low G^* represents the plateau modulus of the diluted long chains of PS-820k with $G_N = G_{Nm}\phi^2 \cong 2.5 \cdot 10^3$ Pa. While the high G^* minimum becomes deeper with the increasing molar mass of the matrix, the low modulus minimum is increasingly shallower due to the slower relaxation of the longer matrix chains. The relaxation modulus $G(t)$ according to Eq. (4) shows a two-step relaxation process (Fig. 3), the first step being associated with the relaxation of the matrix polymer, the second step with the relaxation of the PS-820k chains. The first step is shifted to shorter times with decreasing molar mass of the matrix until it merges with the transition from the glassy state in the case of matrix OS-8.8k. Even though the relaxation of the matrix chains is much faster than the relaxation of the PS-820k chains, the relaxation of the long chains is increasingly slowed down by entanglements with the matrix chains, when going from a matrix of OS-8.8k to PS-73k. This is in line with the Graessley parameter $Gr = Z_L/Z_S^3$ as presented in Table 2. While at large values of Gr relaxation occurs predominantly via constraint release by the short chains, reptation along the tube formed by long and short chains determines increasingly relaxation of the long chains at smaller values of this parameter.

Table 2 Discrete relaxation spectra from mastercurves of G' and G'' at $T_e = T_g + 31.4$ K obtained by IRIS (Winter and Mours 2006)

PS-820k/8.8k		PS-820k/23k		PS-820k/34k		PS-820k/73k	
g_i [Pa]	τ_i [s]	g_i [Pa]	τ_i [s]	g_i [Pa]	τ_i [s]	g_i [Pa]	τ_i [s]
9.571e + 6	3.042e − 4	2.708e + 7	1.922e − 4	1.122e + 8	4.783e − 5	2.933e + 7	2.148e − 4
3.212e + 5	2.120e − 2	6.434e + 5	4.556e − 3	7.100e + 5	4.925e − 3	7.133e + 5	3.898e − 3
1.618e + 5	3.542e − 2	2.734e + 5	2.260e − 2	2.485e + 5	2.579e − 2	3.107e + 5	1.645e − 2
8.389e + 3	3.649e − 1	1.708e + 5	1.328e − 1	1.330e + 5	1.353e − 1	1.736e + 5	7.664e − 2
3.708e + 3	1.686e + 0	5.073e + 4	3.015e − 1	1.417e + 5	6.266e − 1	8.534e + 4	6.008e − 1
1.593e + 3	9.013e + 0	1.091e + 4	1.099e + 0	6.461e + 3	5.783e + 0	5.672e + 4	2.825e + 0
7.174e + 2	4.443e + 1	3.567e + 3	7.791e + 0	2.254e + 3	3.823e + 1	7.452e + 4	8.545e + 0
5.517e + 2	1.606e + 2	1.214e + 3	4.295e + 1	1.128e + 3	3.385e + 2	4.173e + 3	5.916e + 1
6.641e + 2	7.424e + 2	7.751e + 2	2.151e + 2	7.769e + 2	1.786e + 3	1.607e + 3	3.484e + 2
1.177e + 1	1.140e + 4	6.759e + 2	7.957e + 2	3.503e + 1	7.185e + 3	7.852e + 2	2.205e + 3
		2.830e + 2	3.567e + 3			3.610e + 2	6.150e + 3

The extended interchain pressure (EIP) model and the fracture criterion

In the following, we give a short summary of the EIP model and the fracture criterion for monodisperse polymer melts and solutions. For details, we refer to the original publications (Wagner et al. 2021a, 2021b). As we will show, this is sufficient for modeling of the elongational viscosity of the bidisperse blends of PS-820k is considered long as the matrix polymer chains are not stretched.

The extended interchain pressure (EIP) model

The extended interchain pressure (EIP) model for monodisperse polymer melts and solutions is a generalized tube segment model with strain-dependent tube diameter (Wagner

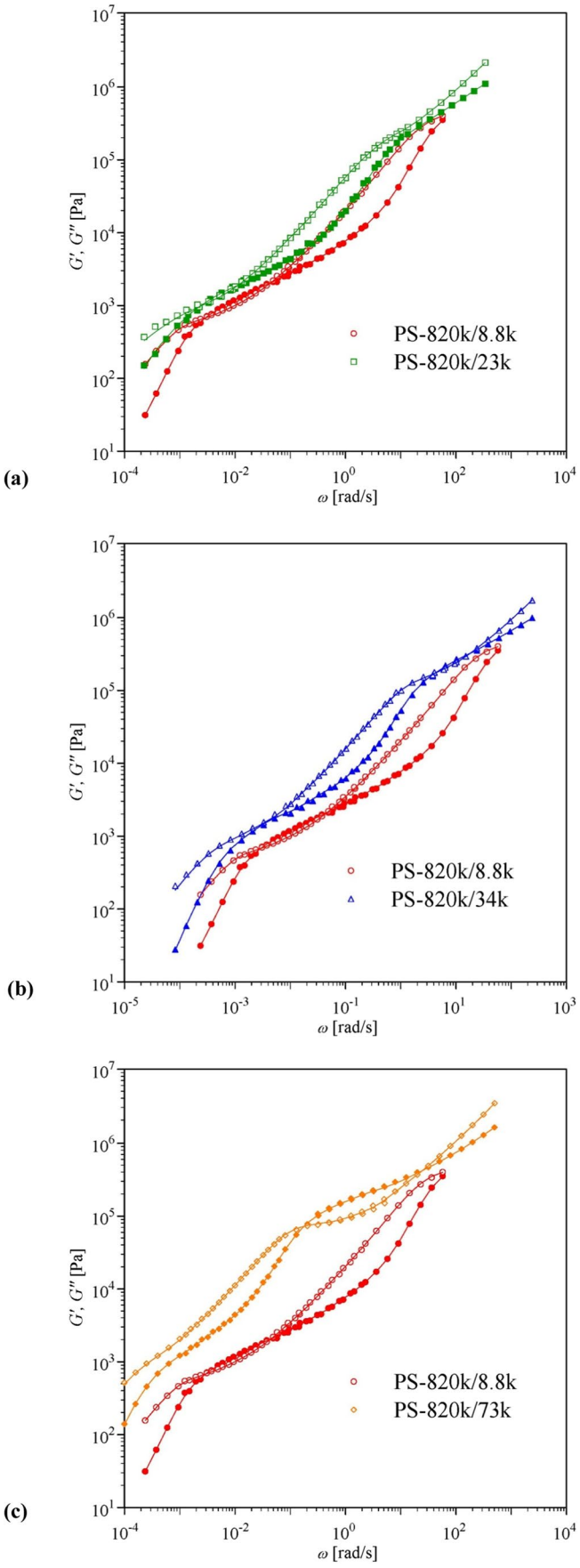

Fig. 1 Comparison of data of G' (full symbols) and G'' (open symbols) and fit (lines) by parsimonious relaxation spectra (Table 2) at $T_e = T_g + 31.4$ K

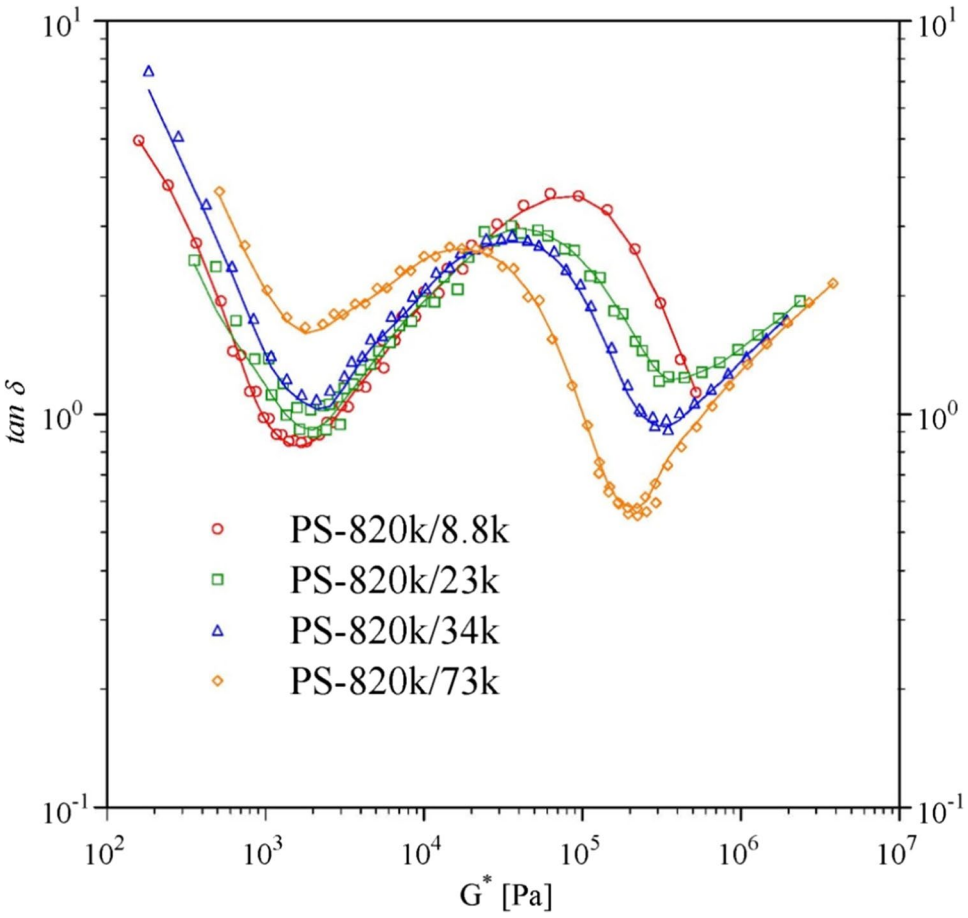

Fig. 2 Comparison of data (symbols) and fit (lines) of loss tangent δ as a function of the absolute value of the complex modulus G^* by parsimonious relaxation spectra (Table 2) at $T_e = T_g + 31.4$ K

1990; Wagner and Schaeffer 1992; Wagner et al. 2001, 2003, 2005; Narimissa et al., 2021). The extra stress tensor $\sigma(t)$ at time t with consideration of finite chain extensibility effects (Rolon-Garrido et al. 2006) is given by a history integral of the form:

$$\sigma(t) = \int \frac{\partial G(t-t')}{\partial t'} f\lambda \; S_{\mathrm{DE}}^{\mathrm{IA}}(t,t')dt' \tag{5}$$

The strain measure $S_{\mathrm{DE}}^{\mathrm{IA}}$ represents the contribution to the extra stress tensor originating from the affine rotation of the tube segments assuming "independent alignment (IA)" (Doi and Edwards 1978, 1979), and is given by

$$S_{\mathrm{DE}}^{\mathrm{IA}}(t,t') \equiv 5\left\langle \frac{u'u'}{u'^2} \right\rangle_{\mathrm{o}} = 5S(t,t') \tag{6}$$

with $S(t,t')$ being the relative second order orientation tensor. $\mathbf{u}'\,\mathbf{u}'$ is the dyad of a deformed unit vector $\underline{\mathbf{u}}' = \underline{\mathbf{u}}'(t, t')$,

$$\underline{\mathbf{u}}' = F_t^{-1} \cdot \mathbf{u} \tag{7}$$

$F_t^{-1} = F_t^{-1}(t,t')$ is the relative deformation gradient tensor and u' is the length of $\mathbf{u}'$. The orientation average is indicated by $<\ldots>_0$,

$$\langle \ldots \rangle_{\mathrm{o}} \equiv \frac{1}{4\pi} \oiint [\ldots] \sin\theta_o d\theta_o d\phi_o \tag{8}$$

i.e., an average over an isotropic distribution of unit vectors $\mathbf{u}$.

$\lambda = \lambda(t,t')$ represents the inverse of the relative tube diameter a/a_0, and also the relative length of a deformed tube segment (Rolon-Garrido et al. 2006),

$$\lambda(t,t') = \frac{a_0}{a(t,t')} = \frac{l(t,t')}{l_0} \tag{9}$$

t' indicates the time when the tube segment was created with equilibrium tube diameter a_0 and equilibrium length l_0.

In the Gaussian limit, the molecular stress function f, i.e., the relative tension in the chain, is equal to the tube stretch λ. However, this is valid only as long as $\lambda << \lambda_{\mathrm{max}}$,

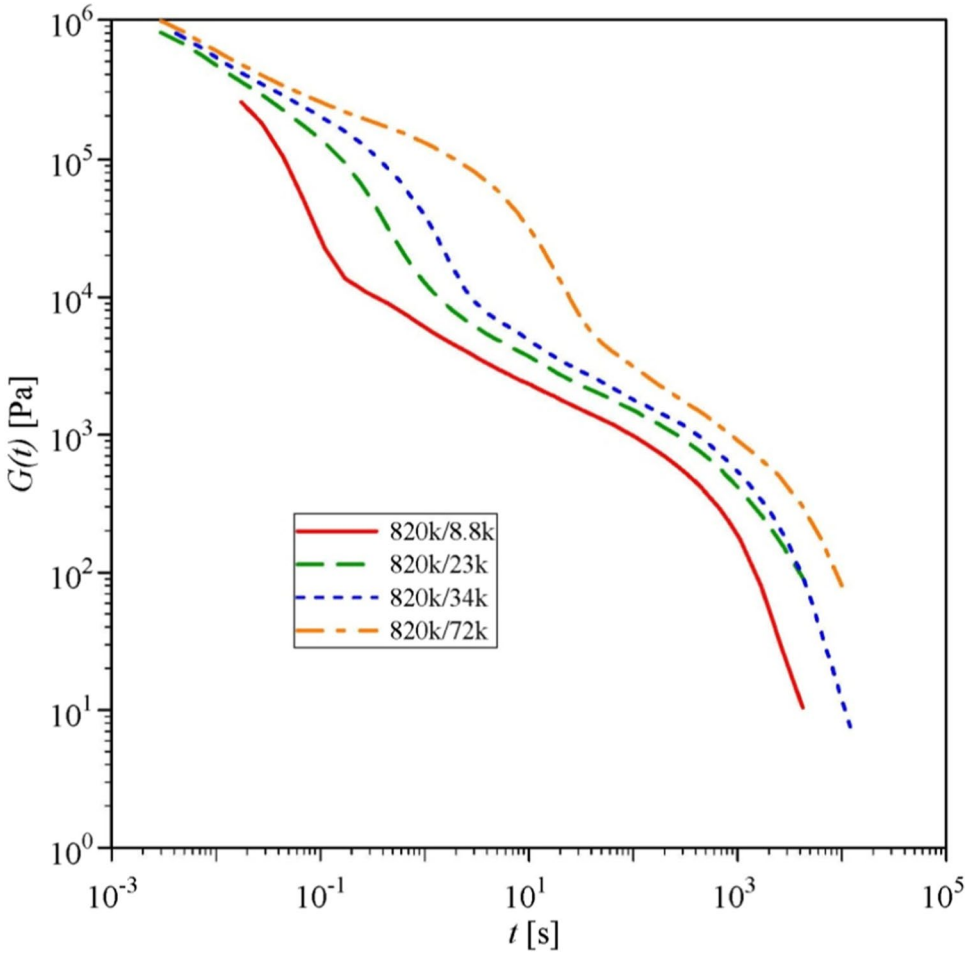

Fig. 3 Relaxation modulus $G(t)$ as a function of time t as calculated from relaxation spectra (Table 2) at $T_e = T_g + 31.4$ K

where $\lambda_{\max} \cong \sqrt{N_e}$ represents the maximum stretch (i.e., a fully extended chain), and N_e the number of Kuhn monomers in an entanglement segment. Nonlinear elasticity caused by finite extensibility (FENE) is implemented in the EIP model in the following way:

$$f = c(\lambda)\lambda \tag{10}$$

c is a nonlinear spring coefficient, representing a relative Padé inverse Langevin function with (Cohen 1991)

$$c = \frac{\left(3 - \frac{\lambda^2}{\lambda_{\max}^2}\right) \cdot \left(1 - \frac{1}{\lambda_{\max}^2}\right)}{\left(3 - \frac{1}{\lambda_{\max}^2}\right) \cdot \left(1 - \frac{\lambda^2}{\lambda_{\max}^2}\right)} \tag{11}$$

In agreement with our earlier work (Wagner et al. 2021a, 2021b), we take the number of Kuhn steps per entanglement in polystyrene melt as $N_{\mathrm{em}} = 21.8$, corresponding to $\lambda_{\max} \cong \sqrt{N_{\mathrm{em}}/\phi} = 14.8$ for a polystyrene solution with a polymer volume fraction of $\phi = 0.1$. While $S_{\mathrm{DE}}^{\mathrm{IA}}$ is determined directly by the deformation history according to Eqs. (6) and (7), λ is found as solution of an evolution equation taking into account affine tube segment deformation balanced by Rouse relaxation and the interchain pressure:

$$\frac{\partial \lambda}{\partial t} = \lambda(\kappa : S) - \frac{\lambda - 1}{\tau_R}\left(1 - \frac{2}{3}\phi^4\right) - \frac{2\phi^4}{9\tau_R}\lambda^2 \quad \left(\lambda f^2 - 1\right) \tag{12}$$

The first term on the right-hand side describes affine deformation with κ being the deformation rate tensor, the second term Rouse relaxation, and the third term represents the interchain pressure contribution (Wagner et al. 2021a, 2021b). We note that the interchain pressure term, which is limiting chain stretch, is proportional to the fourth power of the polymer fraction ϕ, and therefore solutions with lower ϕ show higher maximal stretches. Equation (12) reduces to the evolution equation of the EIP model of Narimissa et al. (2020a) in the Gaussian limit, i.e., when $c = 1$ and $f = \lambda$. Equations (5) and (12) represent the EIP model with finite chain extensibility and are solved numerically.

At high Weissenberg numbers $\mathrm{Wi} = \dot{\varepsilon}\tau_R$ and at large deformations, i.e. when the equilibrium stretch is reached

and therefore $\partial\lambda/\partial t = 0$, it follows from Eq. (12) that the product of molecular stress f and stretch λ is proportional to the square root of Wi and inverse proportional to the square of the polymer fraction:

$$f\lambda = c\lambda^2 = \frac{3}{2}\phi^{-2}\sqrt{2\mathrm{Wi}} \tag{13}$$

and the tensile stress is expected to reach an asymptotic value of

$$\sigma = 5G_N f\lambda = \frac{15}{2}G_N\phi^{-2}\sqrt{2\mathrm{Wi}} \tag{14}$$

From Eq. (14), and considering that $G_N = G_{\mathrm{Nm}}\phi^2$, the universal asymptotic relation for the high Wi tensile stress of melts and solutions of Narimissa et al. (2020a) is recovered

$$\sigma = \frac{15}{2}G_{\mathrm{Nm}}\sqrt{2\mathrm{Wi}} \tag{15}$$

with G_{Nm}being the plateau modulus of the melt.

The fracture criterion

The thermal energy w_{eq} at a temperature T of 403 K (130 °C) is

$$w_{\mathrm{eq}} = 3\,kT = 1.67 \bullet 10^{-20}\mathrm{J} \tag{16}$$

with Boltzmann's constant $k = 1.38 \cdot 10^{-23}$ J/K. On the other hand, the bond dissociation energy of a single carbon-carbon bond in hydrocarbons is (Wagner et al. 2018)

$$U = \frac{348\ \mathrm{kJ}}{N_A} = 5.78 \bullet 10^{-19}\mathrm{J} \cong 35w_{\mathrm{eq}} \tag{17}$$

with Avogadro's number $N_A = 6.02 \times 10^{23}$. Thus, the bond energy U is about 35 times larger than the thermal energy w_{eq} at 130 °C, which is why the polymer chain will not rupture due to Brownian motion at equilibrium.

As explained by Wagner et al. (2021a, 2021b), the strain energy of a chain segment is taken as

$$w\left(N_{\mathrm{em}}\right) = 3kTf\lambda\phi \tag{18}$$

with N_{em} being the number of Kuhn monomers of an entanglement segment in the melt. When the strain energy of the segment reaches the critical energy:

$$w_c = 3kTf_c\lambda_c\phi = U \tag{19}$$

the total strain energy of the chain segment will be concentrated on one C–C bond by thermal fluctuations, and this bond then ruptures. Stretch and tension are relative quantities depending on t and t', and therefore the strain energy$w = w(t,t')$ is also a relative quantity. Chain segments with long relaxation times, i.e., those preferably in the middle of the chain, will be the first to reach the critical energy w_c and will fracture. As soon as the strain energy accumulated between the start-up of deformation and the time $t = t_c$ of fracture reaches the critical energy w_c, a sufficient concentration of locally ruptured chains is reached, and crack initiation will occur. Crack initiation is followed by crack growth, which leads within a very short time (about 200 ms according to Huang et al. 2016b) to brittle fracture of the sample. At time $t = t_c$, the critical Hencky strain at fracture, $\varepsilon_c = \dot{\varepsilon}\ t_c$, is reached and the critical tensile stress at fracture, $\sigma_c = \sigma(t_c)$, is given by the stress equation (5).

From the fracture hypothesis defined by Eq. (19), the maximum achievable product of critical molecular stress f_c and critical stretch λ_c is obtained (Wagner et al. 2021a, 2021b),

$$f_c\lambda_c\phi = c\lambda_c^2\phi = \frac{U}{3kT} \cong 35 \tag{20}$$

We called this fracture mode "entropic fracture" (Wagner et al. 2018), as it is caused by thermal fluctuations, in contrast to the "enthalpic fracture" hypothesis of Lake and Thomas (1967) as modified by Mazich and Samus (1990). These authors assumed that all bonds are fully stretched at fracture and when a chain with N C–C bonds between two entanglement points ruptures, the strain energy $w_c = \mathrm{NU}$ corresponding to the bond energy of all N C–C bonds in the entangled chain segment is dissipated.

Combining the fracture criterion of Eq. (20) with the asymptotic tensile stress at high Wi and large stretch according to Eq. (14), we expect at sufficiently fast and large elongations an asymptotic critical tensile stress σ_c at fracture,

$$\sigma_c = 5G_N f_c\lambda_c = \frac{15}{2}G_N\phi^{-2}\sqrt{2\mathrm{Wi}_c} \cong 5G_N\frac{U}{3\mathrm{kT}}\phi^{-1} \tag{21}$$

From the first and last term of this identity and considering that $G_N = G_{\mathrm{Nm}}\phi^2$, the asymptotic critical stress σ_c is obtained as

$$\sigma_c = 5G_{\mathrm{Nm}}\phi\frac{U}{3kT} \cong 175G_{\mathrm{Nm}}\phi \tag{22}$$

For $\phi = 0.1$ and taking the plateau modulus of polystyrene melt as $G_{\mathrm{Nm}} = 2.5 \cdot 10^5$ Pa (Wagner et al. 2021a, 2021b), the asymptotic critical elongational stress growth coefficient η_{Ec}^+ at fracture is given by

$$\eta_{\mathrm{Ec}}^+(\dot{\varepsilon}) \cong \frac{175G_{\mathrm{Nm}}\phi}{\dot{\varepsilon}} = \frac{4.4 \cdot 10^6}{\dot{\varepsilon}}\mathrm{Pa\ s} \tag{23}$$

The reduced critical Weissenberg number Wi_c for the onset of fracture

$$\mathrm{Wi}_c = \frac{2}{9}\left(\frac{U}{3\mathrm{kT}}\phi\right)^2 \cong 272\phi^2 \tag{24}$$

is obtained from the two last terms of Eq. (21). Wi_c is the minimum Weissenberg number for fracture to occur, i.e., fracture is expected only for $Wi \geq Wi_c$. For $\phi = 0.1$ and the Rouse time $\tau_R = 359$ s of PS-820k (Table 1), the critical elongation rate $\dot{\varepsilon}_c$ for the onset of fracture is given by:

$$\dot{\varepsilon}_c \cong \frac{272\phi^2}{\tau_R} = 0.008 \ \ s^{-1} \tag{25}$$

Thus, according to the fracture criterion, in the asymptotic limit of Eq. (21) fracture is expected to occur for $\dot{\varepsilon} \geq 0.008 \ \ s^{-1} \cong 0.01 \ \ s^{-1}$.

Comparison of experimental data and model predictions

In the following, we compare predictions of the extended interchain pressure (EIP) model, Eqs. (5) and (12), and the fracture criterion, Eq. (20), with experimental evidence. Figure 4 presents the elongational stress growth coefficient $\eta_E^+(t)$ as a function of time t for solution PS-820k/8.8k. Excellent agreement of data and predictions is seen for the elongational stress growth coefficient, where predictions and experimental data are nearly indistinguishable, except at the lowest strain rate of 0.003 s^{-1}. We note that the prediction for low strain rates is very sensitive to the long-time tail of the relaxation spectrum, which might not have been fully resolved by mechanical spectroscopy. While at elongation rates of 0.003 and 0.01 s^{-1}, a steady-state elongational viscosity is predicted, filament rupture at an elongation rate of 0.2 s^{-1} is evident. The elongational stress growth coefficient at elongation rates of 0.03 and 0.06 s^{-1} shows a maximum and then a drop of the viscosity, which may be interpreted as a delayed fracture. At elongation rates of 0.09 and 0.01 s^{-1} there is an indication of necking, i.e., above a certain deformation, the elongational stress growth coefficient $\eta_E^+(t)$ shows a distinctive kink to a lower slope of $\eta_E^+(t)$ before the filament finally fails.

The fracture criterion of Eq (20) is found to be in general agreement with experimental evidence, and fracture is seen to occur at elongation rates of $\dot{\varepsilon} > 0.01 \ \ s^{-1}$ in agreement with Eq. (25) predicting that fracture occurs at elongation rates $\dot{\varepsilon} \geq 0.01 \ \ s^{-1}$. Figure 4 shows the asymptotic critical stress growth coefficient η_{Ec}^+ at fracture according to Eq. (23). The asymptotic state of η_{Ec}^+ predicted is reached

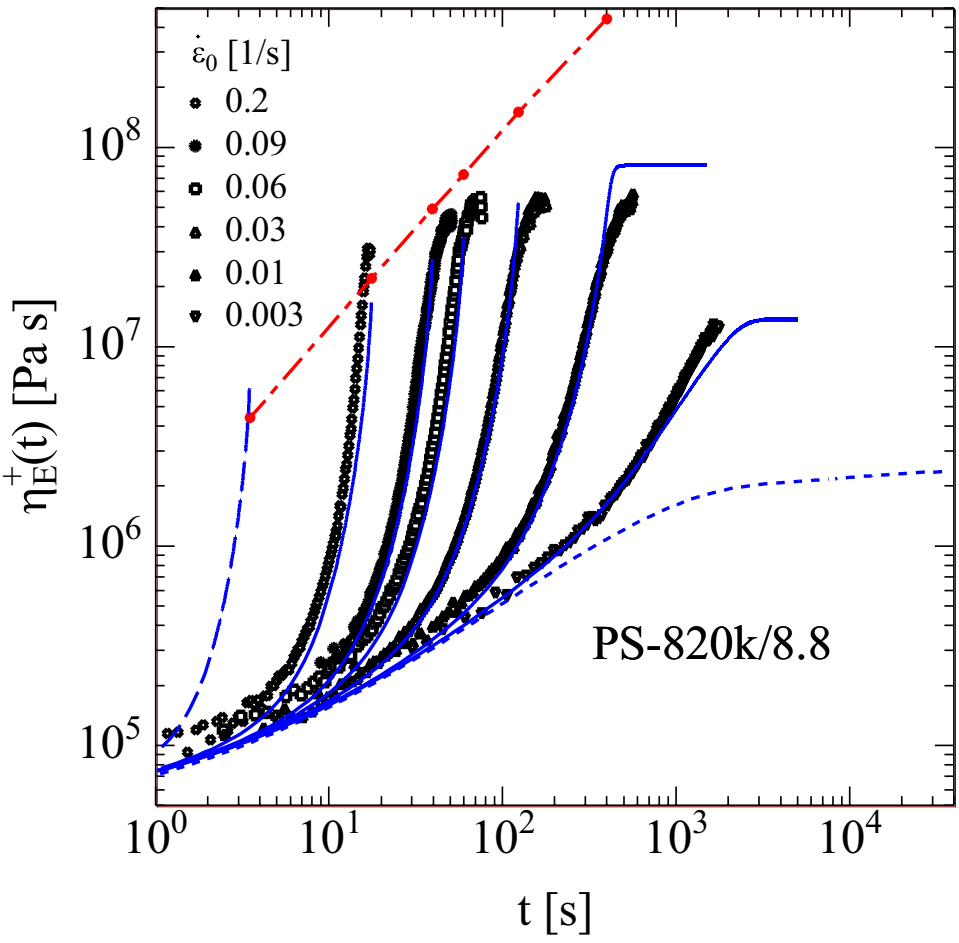

Fig. 4 Comparison of data (symbols) and predictions (lines) of elongational stress growth coefficient $\eta_E^+(t)$ for blend PS-820k/8.8k at T_e = 130 °C. Short dotted line is prediction of $\eta_E^0(t)$, long dotted line is prediction of $\eta_E^+(t)$ for $\dot{\varepsilon} = 1 \ \ s^{-1}$. Short-long dotted line with dots indicates the asymptotic elongational stress growth coefficient η_{Ec}^+ at fracture according to Eq. (23)

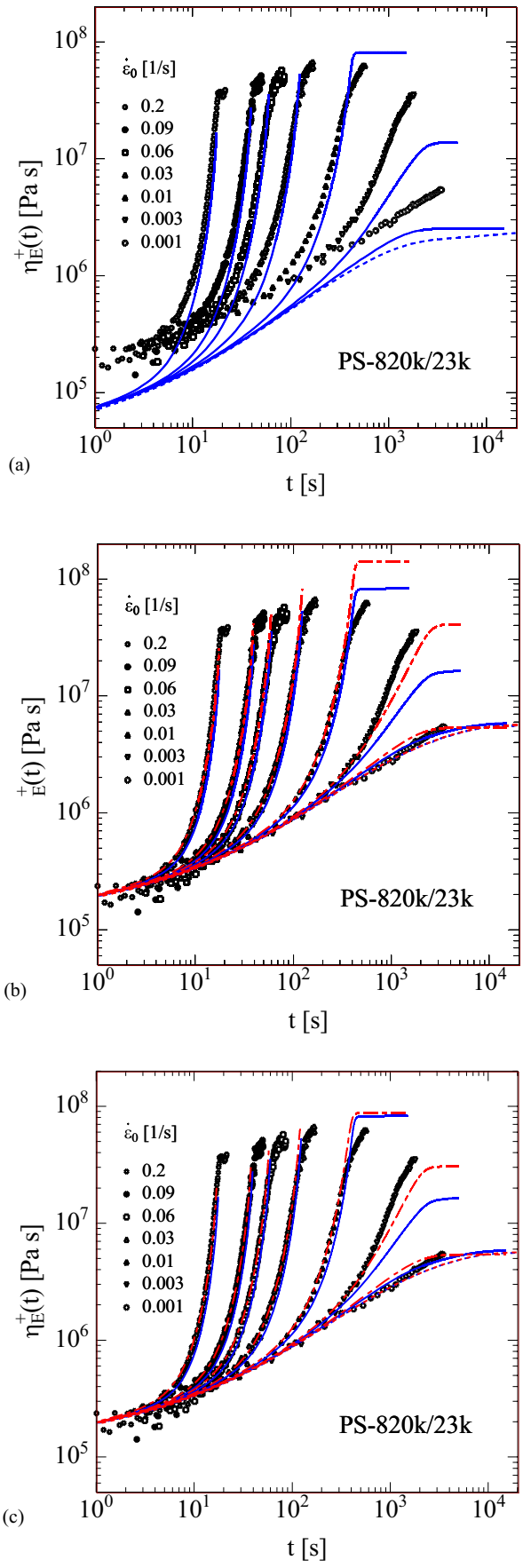

Fig. 5 Comparison of data (symbols) and predictions (lines) of elongational stress growth coefficient $\eta_E^+(t)$ for blend PS-820k/23k at T_e = 135 °C. Short dotted lines are predications of $\eta_E^0(t)$. **a** Full lines are predictions for PS-820k/8.8k from Eqs. (5) and (12); **b** and **c** full lines are predictions for PS-820k/23k from Eq. (26); long-short dotted lines are predictions of Eqs. (5), (12), and (20) with relaxation spectrum of PS-820k/23k; $\phi = 0.1$ (**b**) and $\phi_{\text{eff}} = 0.13$(**c**)

at $\dot{\varepsilon} > 0.1\ \ s^{-1}$, while at lower elongation rates, the stress growth coefficient is smaller due to relaxation processes. We conclude that for PS-820k/8.8k, data and predictions of the EIP model including the fracture criterion are in agreement with experimental accuracy, and we note that this modeling is based exclusively on linear-viscoelastic characterization, the Rouse time of PS-829k, and the ratio of strain energy to thermal energy.

The data of the elongational stress growth coefficient $\eta_E^+(t)$ as a function of time t for blend PS-820k/23k are shown in Fig. 5. Comparison of data at T_e = 135 °C and predictions of the EIP model for PS-820k/8.8k at T_e = 130 °C are presented in Fig. 5a. This comparison is possible as solution PS-820k/8.8k and blend PS-820k/23k were measured at iso-T_g conditions and therefore the Rouse time of the long chains in both matrices is exactly the same (Wagner 2014, Shahid et al 2019). Good agreement of data and predictions is seen for the elongational stress growth coefficient at higher strains, while the linear-viscoelastic start-up of data and predictions disagrees considerably because of the higher matrix viscosity of PS23k in comparison to OS8.8k. As suggested by Shahid et al. (2021), the early stretching of the long chains of PS-820k may be masked by the linear-viscoelastic contribution of the matrix chains of PS-23k. We take this difference in the linear-viscoelastic start-up of the elongational viscosities simplistically into account by adding the LVE contribution of PS-820k/M with M = *23* k to the $\eta_E^+(t)$ prediction of PS-820k/8.8k, followed by subtracting the LVE contribution of PS-820k/8.8k, i.e.,

$$\eta_E^+(t) = \eta_E^+(\text{PS}-820\text{k}/8.8\text{k}) + \eta_E^0(\text{PS}-820\text{k}/M) - \eta_E^0(\text{PS}-820k/8.8\text{k}) \tag{26}$$

$\eta_E^+(\text{PS}-820\text{k}/8.8\text{k})$ is the elongational stress growth coefficient of PS-820k/8.8k based on the relaxation time spectrum of PS-820k/8.8k as presented in Fig. 1, and the LVE contributions η_E^0 are given by

$$\eta_E^0(\text{PS}-820\text{k}/M) = 3\sum_i g_i\tau_i\left(1-\exp\left(-t/\tau_i\right)\right) \tag{27}$$

with partial moduli $g_i$and relaxation times τ_i for the blend PS-820k/M (with M = 23 k) and the solution PS-820k/8.8k (PS-820k/M with M = 8.8 k) as given in Table 2. We call Eq. (26) modeling approach "A" in the following.

When accounting for the difference in the LVE behaviors of PS820k/23k and PS-820k/8.8k using Eq. (26), good agreement between data of PS-820k/23k with not only the LVE predictions but also with the elongational stress growth coefficient $\eta_E^+(t)$ at all strains is obtained (full lines in Fig. 5b and 5c), except at the strain rate of 0.003 s^{-1}. We note also that the predictions of the stress growth coefficient are slightly shifted to the right of the data. These effects will become more significant with increasing molar mass of the matrix as shown below. It is a consequence of the fact that the relaxation of the long chains is slowed down by the short chains as shown in Fig. 3, and therefore the relaxation time spectrum of blend PS-820k/23k has an enhanced long-time tail compared to PS-820k/8.8k.

Instead of correcting the LVE behavior by use of Eq. (27), we take alternatively the linear-viscoelastic interactions between the long chains of PS-820k and the matrix chains of PS-23k into account and use the spectrum of PS-820k/23k in the stress equation (5). Excellent agreement of data and predictions of the elongational stress growth coefficient for $\dot{\varepsilon} \geq 0.01\ s^{-1}$ is obtained, and agreement for $\dot{\varepsilon} = 0.003\ s^{-1}$ is much improved (Fig. 5b). However, the steady-state elongational viscosity at $\dot{\varepsilon} = 0.01\ s^{-1}$ is now overpredicted. This is due to the increased number of entanglements along the PS-820k chains, which are not only formed by entanglements of long chains with themselves, but also by interactions of long and short chains. According to the EIP model, an increased number of entanglements will lead to enhanced interchain pressure limiting maximal stretch (Narimissa et al. 2020a). We quantify the effect of the entanglements formed by the matrix polymer along the long chains of PS-820k in the following way: From Eq. (1) the total number of entanglements of a test chain of PS-820k is $Z_L = M_L/M_e$ in the melt state, largely independent of the matrix as long as the matrix chains are long enough to be entangled. The number of entanglements of the test chain with other long chains is from Eq. (2) $Z_{LL} = \phi Z_L$, while the number of short chains being entangled with the test chain is given by $Z_{LS} = (1-\phi) Z_L$. The total mass of the matrix chains with molar mass M_S being entangled with the test chain is therefore $M_{LS} = (1-\phi) Z_L M_S$. We make the assumption that the effect of entanglements of the test chain with the matrix chains on the interchain pressure can be represented by an equivalent number Z_P of pseudo-PS-820k chains with the same total molar mass as the total molar mass of the short chains, i.e., $Z_P M_L \equiv M_{LS} = (1-\phi) Z_L M_S$. Thus, the total number of effective entanglements of the test chain is $Z_{eff} = Z_{LL} + Z_P = Z_L[\phi + (1-\phi) M_S/M_L]$, and the effective polymer fraction of PS-820k, $\phi_{eff} = Z_{eff}/Z_L$, is given by

$$\phi_{eff} = \phi + (1-\phi) M_S/M_L \tag{28}$$

We take this effect of an increased number of entanglements of the long chains into account by replacing the polymer fraction $\phi = 0.1$ in the stretch equation (12) and in the fracture criterion (20) by the effective polymer fraction $\phi_{eff} \geq 0.1$ of Eq. (28) and call this modeling approach "B". Equation (28) constitutes a linear mixing rule which does not depend on the entanglement molar mass M_e, and features the correct asymptotic values of $\phi_{eff} = 1$ for $M_S = M_L$, i.e., when the "matrix" consists of long chains, and $\phi_{eff} = \phi$ for $M_S \to 0$, i.e., when the matrix is not entangled, such as in the case of OS-8.8k. For matrix PS-23k, Eq. (28) results in a value of $\phi_{eff} = 0.13$, and nearly quantitative agreement of data and predictions is achieved as shown in Fig. 5c. We note that the exact value of the polymer fraction has only an insignificant influence on the elongational stress growth coefficient, which is largely independent of ϕ as seen by comparing the start-up viscosities of Fig. 5b to 5c. The interchain pressure term in the stretch Eq. (12) has only an effect at large stretches, and together with the fracture criterion of Eq. (20) determines the value of the maximal elongational viscosity.

Similarly, the data of the elongational stress growth coefficient $\eta_E^+(t)$ as a function of time t for blend PS-820k/34k are shown in Fig. 6a. The data are in good agreement with predictions of the EIP model for PS-820l/8.8k at higher strains, while the disagreement of LVE data and predictions increases further due to the higher matrix viscosity of PS34k compared to OS8.8k. When taking the difference in the LVE behaviors of PS820k/34k and PS-820k/8.8k into account by Eq. (26) with $\eta_E^0(PS-820k/M) = \eta_E^0(PS-820k/34k)$ (model approach A), good agreement between data of PS-820k/34k and predictions is again obtained for the elongational stress growth coefficient $\eta_E^+(t)$, except at the strain rate 0.003 s^{-1} (Fig. 6b and 6c). Again we note that predictions are shifted to the right of the experimental data.

Modeling approach B, i.e., using the spectrum of PS-820k/34k in the stress equation (5) results in the excellent agreement of data and predictions for the elongational stress growth coefficient for $\dot{\varepsilon} \geq 0.01\ s^{-1}$, where predictions (long-short dotted lines) go through the experimental data, and improved agreement for $\dot{\varepsilon} = 0.003\ s^{-1}$ (Fig. 6b). But again, the steady-state viscosity at $\dot{\varepsilon} = 0.01\ s^{-1}$ is significantly overpredicted. When replacing the polymer fraction $\phi = 0.1$ in the stretch equation (12) as well as in the fracture criterion (20) by the effective polymer fraction of $\phi_{eff} = 0.14$ as obtained from Eq. (28), nearly quantitative agreement of data and predictions is achieved within experimental accuracy (Fig. 6c).

Comparison of data (symbols) and predictions (lines) of the elongational stress growth coefficient $\eta_E^+(t)$ for blend PS-820k/73k are shown in Fig. 7. Although there is a large discrepancy between data of PS-820k/73k and predictions for PS-820k/8.8k in the LVE and the start-up regime, qualitative agreement of data and predictions is

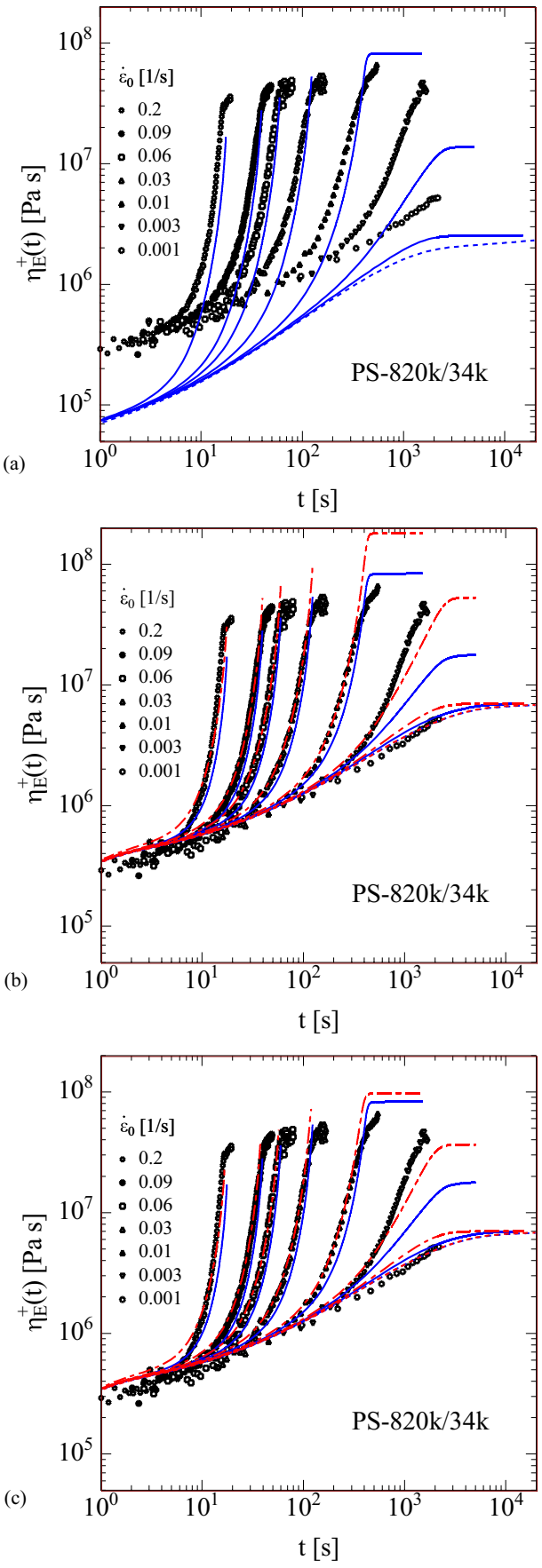

Fig. 6 Comparison of data (symbols) and predictions (lines) of elongational stress growth coefficient $\eta_E^+(t)$for blend PS-820k/34k at T_e = 136 °C. Short dotted line is predication of $\eta_E^0(t)$. **a** Full lines are predictions for PS-820k/8.8k from Eqs. (5) and (12); **b** and **c** full lines are predictions for PS-820k/34k from Eq. (26); long-short dotted lines are predictions of Eqs. (5), (12), and (20) with relaxation spectrum of PS-820k/23; $\phi = 0.1$ (**b**) and $\phi_{eff} = 0.14$(**c**)

still observed at higher strains (Fig. 7a). Modeling approach A, i.e., accounting for the difference in the LVE behaviors of PS820k/73k and PS-820k/8.8k by use of Eq. (26) with $\eta_E^0(\mathrm{PS}-820\mathrm{k}/M) = \eta_E^0(\mathrm{PS}-820\mathrm{k}/73\mathrm{k})$, leads to largely improved agreement of data and predictions except at the strain rate of 0.003 s^{-1} (Fig. 7b and 7c). Modeling approach B, i.e., using the spectrum of PS-820k/73k in the stress equation (5) results in excellent agreement of data and predictions for the elongational stress growth coefficient at elongational rates of 0.06 $s^{-1} \geq \dot{\varepsilon} \geq 0.01$ s^{-1} and qualitative agreement for $\dot{\varepsilon} = 0.003$ s^{-1} and $\dot{\varepsilon} \geq 0.09$ s^{-1} (Fig. 7b), but the maxima of the elongational stress growth coefficient are strongly overpredicted. When replacing the polymer fraction $\phi = 0.1$ in the stretch equation (12) and in the fracture criterion (20) by an effective polymer fraction of $\phi_{eff} = 0.18$resulting from Eq. (28), improved agreement of data and predictions is achieved (Fig. 7c). For $\dot{\varepsilon} \geq 0.09$ s^{-1}, strain hardening is predicted to start significantly earlier than observed experimentally, which is related to the stretching of the matrix chains as expected for $\mathrm{Wi} \geq 1/3$ corresponding to $\dot{\varepsilon} \geq 0.1$ s^{-1}.

Conclusion

The elongational viscosity data of a well-characterized set of bidisperse polystyrene blends consisting of 10% mass fraction of monodisperse polystyrene PS-820k (molar mass of 820 kg/mol) and 90% matrix polystyrene with molar masses of 8.8, 23, 34, and 73 kg/mol, respectively, were analyzed by the extended interchain pressure (EIP) model along with the finite chain extensibility and entropic fracture criterion for brittle fracture of polymer systems (Wagner et al. 2021a, 2021b). Modeling based exclusively on the linear-viscoelastic characterization of PS820k/8.8k, the Rouse time of PS-820k, and the ratio between strain energy and thermal energy results in general agreement of experimental data and predictions of the maximal viscosity, and confirms the qualitative conclusions of Shahid et al. (2021) that strain hardening of the blends is mainly determined by the stretching of the PS-820k chains in the experimental window, independent of the molar mass of the matrix. The same behavior was observed earlier by Nielsen et al. (2008) for two blends of 14% PS390k (390 kg/mol) with either 86% of PS50k (50 kg/mol) or 86% of PS100k (100 kg/mol). Both blends, PS390k/50k and PS390k/100k show the same steady-state

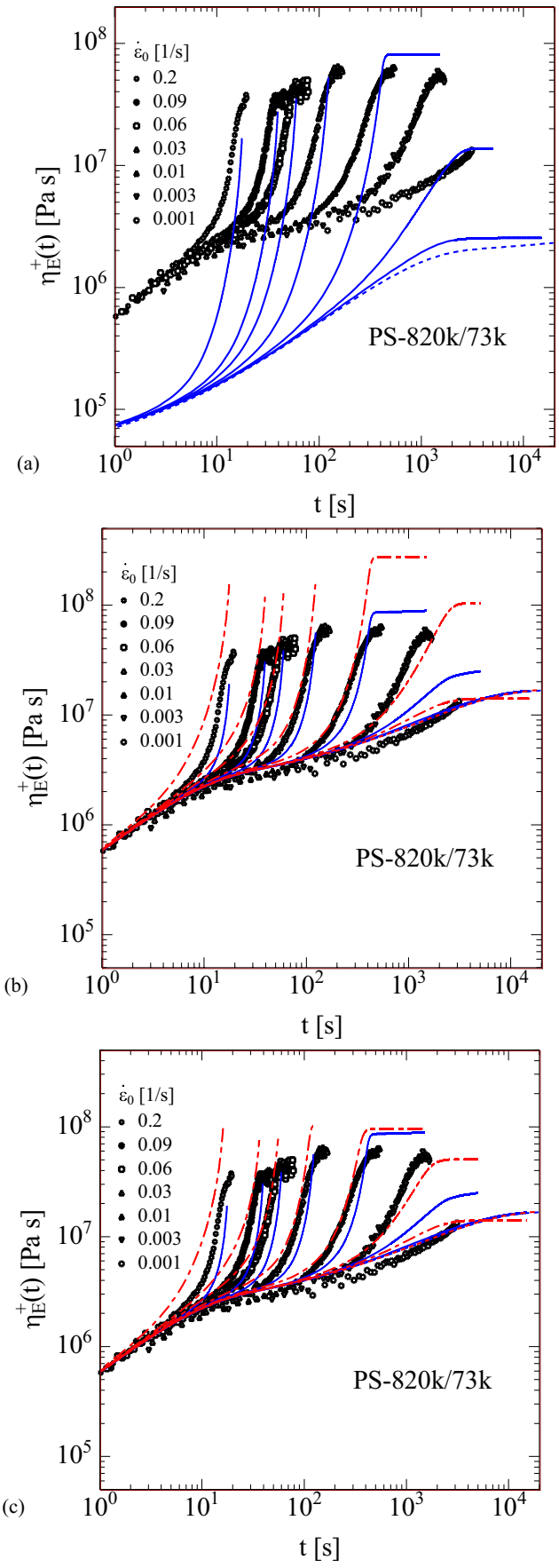

Fig. 7 Comparison of data (symbols) and predictions (lines) of elongational stress growth coefficient $\eta^+_E(t)$ for blend PS-820k/73k at T_e = 138 °C. Short dotted line is predication of $\eta^0_E(t)$. **a** Full lines are predictions for PS-820k/8.8k from Eqs. (5) and (12); **b** and **c** full lines are predictions for PS-820k/73k from Eq. (26); long-short dotted lines are predictions of Eqs. (5), (12), and (20) with relaxation spectrum of PS-820k/73k; $\phi = 0.1$ (**b**) and $\phi_{\text{eff}} = 0.18$(**c**)

elongational viscosity at sufficiently large $\dot{\varepsilon}$, which is obviously determined by the stretching of the high molar mass chains of PS390k, while the start-up behavior is influenced by the different linear-viscoelastic extensional stress growth coefficients of PS50k and PS100k (see Fig. 3 of Narimissa et al. 2020a). For the bidisperse blends of PS-820k and lower molar mass polystyrenes investigated here, the simple addition/subtraction of $\eta^0_E(t)$ according to Eq. (26) of the modeling approach A has no effect on the stretching of the long chains but results in good (though not quantitative) agreement of experiments and predictions of the elongational stress growth coefficient. This confirms the conjecture of Shahid et al. (2021) that early stretching of the long chains of PS-820k is masked by the linear-viscoelastic contribution of the matrix chains.

In contrast to modeling approach A, which corrects only the linear-viscoelastic start-up of the blends, but uses the spectrum of PS-820k/8.8k for calculation of the nonlinear viscoelastic behavior of the long chains, modeling approach B takes into account the linear-viscoelastic interaction of long (PS820k) and short chains (PS23k, PS34k, and PS73k) by use of the corresponding relaxation spectra of the blends in the stress equation (5). The additional entanglements between long and short chains result in longer relaxation times of the long chains as shown in Fig. 3, and this has a considerable influence on the nonlinear elongational behavior especially at the lowest elongation rate of 0.003 s^{-1}. However, the linear-viscoelastic long-short chain interactions lead also to a small but significant improvement of the predictions of the elongational stress growth coefficient at higher elongation rates with predictions using modeling approach B being in excellent quantitative agreement with the experimental data. At higher stretches, the higher interchain pressure caused by the additional long-short entanglements limits maximal stretch of the long chains, and consequently similar maximal viscosities as for approach A are obtained. The additional entanglements of the long chains with the shorter matrix chains have a similar effect on the maximal stretch as a larger fraction of long chains in the binary blends, and this effect is larger for longer matrix chains. We quantified the enhanced interchain pressure by introducing an effective polymer fraction $\phi_{\text{eff}} \geq 0.1$ by a linear mixing rule according to Eq. (28), which results in $\phi_{\text{eff}} = 0.13$ for PS820k/23k, $\phi_{\text{eff}} = 0.14$ for PS820k/34k, and $\phi_{\text{eff}} = 0.18$ for PS820k/73k. The limit of modeling approach B is reached when stretching of the matrix chains

starts at $Wi \geq 1/3$ corresponding to $\dot{\epsilon} \geq 0.1\ \text{s}^{-1}$ for blend PS-820k/73k. For larger Wi, the stretching of both the long chains and the short matrix chains has to be considered, with is outside the scope of this work.

This analysis also extends earlier findings of the suitability of the EIP model and the entropic fracture criterion for the modeling of the rheology and failure of monodisperse polymer melts and solutions (Wagner et al. 2021a, 2021b) to bidisperse blends of a high and lower mass polystyrenes as long as the lower mass matrix polymer is not stretched in elongational flow. The essential features of the EIP model and the fracture criterion are (1) nonlinear reptation dynamics is modeled by a history integral of coupled stretch and orientation of temporary entanglement segments, thus avoiding pre-averaging of stretch and orientation (Narimissa and Wagner 2019); (2) stretch and stretch relaxation of entanglement segments are accounted for by an evolution equation of the tube diameter, which includes the effects of affine deformation, Rouse relaxation, and interchain pressure. Both Rouse relaxation and interchain pressure are governed by the Rouse time; (3) when the strain energy of a chain segment reaches the bond energy U of one carbon-carbon bond, the chain fractures and the polymer filament fail by chain scission. Chain segments with long relaxation times, i.e., those preferably in the middle of the chain, will be the first to reach the critical energy and will fracture. Chain segments closer to the ends of the chain, which due to reptation processes have shorter relaxation times and see less stretch and tension are less likely to fracture. For bidisperse polystyrene blends consisting of a 10% mass fraction of monodisperse polystyrene PS-820k, the critical elongation rate for the onset of fracture is predicted to be $\dot{\epsilon}_c \geq 0.008\ \text{s}^{-1}$. This critical value, as well as the stress growth coefficients at fracture agree with experimental evidence within experimental accuracy.

Acknowledgements We are grateful to Evelyne van Ruymbeke and Alexis André for their technical support and helpful discussions during the preparation of this paper.

References

André A, Shahid T, Oosterlinck F, Clasen C, van Ruymbeke E (2021) Investigating the transition between polymer melts and solutions in non-linear elongational flow. Macromolecules 54:2797–2810

Bach A, Almdal K, Rasmussen HK, Hassager O (2003) Elogational viscosity of narrow molar mass distribution polystyrene. Macromolecules 36:5174–5179

Ballauf M, Wolf BA (1984) Degradation of chain molecules. 2. Thermodynamically induced shear degradation of dissolved polystyrene. Macromolecules 17:209–216

Cohen A (1991) A Padé approximant to the inverse Langevin function. Rheol Acta 30:270–273

Doi M, Edwards SF (1978) Dynamics of concentrated polymer systems. Part 3.- The constitutive equation. J Chem Soc Faraday Trans 74:1818–1832

Doi M, Edwards SF (1979) Dynamics of concentrated polymer systems. Part 4.- Rheological properties. J Chem Soc Faraday Trans 75:38–54

Huang Q (2019) Exploring the mechanism of fracture for entangled polymer liquids in extensional flow. Phys Fluids 31:083105

Huang Q, Hassager O (2017) Polymer liquids fracture like solids. Soft Matter 13:3470–3474

Huang Q, Mednova O, Rasmussen HK, Alvarez NJ, Skov AL, Almdal K, Hassager O (2013a) Concentrated polymer solutions are different from melts: role of entanglement molecular weight. Macromolecules 46:5026–5035

Huang Q, Alvarez NJ, Matsumiya Y, Rasmussen HK, Watanabe H, Hassager O (2013b) Extensional rheology of entangled polystyrene solutions suggests importance of nematic interactions. ACS Macro Lett 2:741–744

Huang Q, Hengeller L, Alvarez NJ, Hassager O (2015) Bridging the gap between polymer melts and solutions in extensional rheology. Macromolecules 48:4158–4163

Huang Q, Mangnus M, Alvarez NJ, Koopmans R, Hassager O (2016a) A new look at extensional rheology of low-density polyethylene. Rheol Acta 55:343–350

Huang Q, Alvarez NJ, Shabbir A, Hassager O (2016b) Multiple cracks propagate simultaneously in polymer liquids in tension. Phys Rev Lett 117:087801

Ianniruberto G, Brasiello A, Marrucci G (2012) Simulations of fast shear flows of PS oligomers confirm monomeric friction reduction in fast elongational flows of monodisperse PS melts as indicated by rheooptical data. Macromolecules 45:8058–8066

Ianniruberto G, Marrucci G, Masubuchi Y (2020) Melts of linear polymers in fast flows. Macromolecules 53:5023–5033

Lake GJ, Thomas AG (1967) The strength of highly elastic materials. Proc R Soc Lond A 300:108–119

Malkin AY, Petrie C (1997) Some conditions for rupture of polymer liquids in extension. J Rheol 41:1–25

Marrucci G, Ianniruberto G (2004) Interchain pressure effect in extensional flows of entangled polymer melts. Macromolecules 37:3934–3942

Mazich KA, Samus M (1990) Role of entanglement couplings in threshold fracture of a rubber network. Macromolecules 23:2478–2483

Narimissa E, Wagner MH (2019) Review on tube model based constitutive equations for polydisperse linear and long-chain branched polymer melts. J Rheol 63:361–375

Narimissa E, Huang Q, Wagner MH (2020a) Elongational rheology of polystyrene melts and solutions: concentration dependence of the interchain tube pressure effect. J Rheol 64:95–110

Narimissa E, Schweizer T, Wagner MH (2020b) A constitutive analysis of nonlinear shear flow. Rheol Acta 59:487–506

Narimissa E, Poh L, Wagner MH (2021) Elongational viscosity scaling of polymer melts with different chemical constituents. Rheol Acta 60:163–174
Nielsen JK, Rasmussen HK, Hassager O, McKinley GH (2008) Elongational viscosity of monodisperse and bidisperse polystyrene melts. J Rheol 50:453–476
Rolon-Garrido VH, Wagner MH, Luap C, Schweizer T (2006) Modeling non-Gaussian extensibility effects in elongation of nearly monodisperse polystyrene melts. J Rheol 50:327–340
Shahid T (2018). Understanding and modelling the extensional rheology of nearly monodisperse linear polymers. PhD Thesis KU Leuven, Belgium (http://hdl.handle.net/2078.1/203674)
Shahid T, Clasen C, Oosterlinck F, van Ruymbeke E (2019) Diluting entangled polymers affects transient hardening but not their steady elongational viscosity. Macromolecules 52:2521–2530
Struglinski MJ, Graessley WW (1985) Effects of polydispersity on the linear viscoelastic properties of entangled polymers, part 1: experimental observations for binary mixtures of linear polybutadienes. Macromolecules 18:2630–2643
Wagner MH (1990) The nonlinear strain measure of polyisobutylene melt in general biaxial flow and its comparison to the Doi-Edwards model. Rheol Acta 29:594–603
Wagner MH (2011) The effect of dynamic tube dilation on chain stretch in nonlinear polymer melt rheology. J Non-Newtonian Fluid Mech 166:915–924
Wagner MH (2014) Scaling relations for elongational flow of polystyrene melts and concentrated solutions of polystyrene in oligomeric styrene. Rheol Acta 53:765–777
Wagner MH (2015) An extended interchain tube pressure model for elongational flow of polystyrene melts and concentrated solutions. J Non-Newtonian Fluid Mech 222:121–131
Wagner MH, Rolón-Garrido VH (2009a) Nonlinear rheology of linear polymer melts: modeling chain stretch by interchain tube pressure and Rouse time. Korea-Australia Rheolology J 21:203–211
Wagner MH, Rolón-Garrido VH (2009b) Recent advances in constitutive modeling of polymer melts. Novel Trends of Rheology III. AIP Conf Proc 1152:16–31. https://doi.org/10.1063/1.3203266
Wagner MH, Schaeffer J (1992) Nonlinear measures for general biaxial extension of polymer melts. J Rheol 36:1–26
Wagner MH, Rubio P, Bastian H (2001) The molecular stress function model for polydisperse polymer melts with dissipative convective constraint release. J Rheol 45:1387–1412
Wagner MH, Yamaguchi M, Takahashi M (2003) Quantitative assessment of strain hardening of low-density polyethylene melts by the molecular stress function model. J Rheol 47:779–793
Wagner MH, Kheirandish S, Hassager O (2005) Quantitative prediction of transient and steady-state elongational viscosity of nearly monodisperse polystyrene melts. J Rheol 49:1317–1327
Wagner MH, Narimissa E, Rolon-Garrido VH (2015) From melt to solution: scaling relations for concentrated polystyrene solutions. J Rheol 59:1113–1130
Wagner MH, Narimissa E, Huang Q (2018) On the origin of brittle fracture of entangled polymer solutions and melts. J Rheol 62:221–223
Wagner MH, Narimissa E, Huang Q (2021a) Scaling relations for brittle fracture of entangled polystyrene melts and solutions in elongational flow. J Rheol 65:311–324
Wagner MH, Narimissa E, Poh L, Shahid T (2021b) Modelling elongational viscosity and brittle fracture of polystyrene solutions. Rheol Acta 60:385–396
Winter HH, Mours M (2006) The cyber infrastructure initiative for rheology. Rheol Acta 45:331–338
Yaoita T, Isaki T, Masubuchi Y, Watanabe H, Ianniruberto G, Marrucci G (2012) Primitive chain network simulation of elongational flows of entangled linear chains: stretch/orientation induced reduction of monomeric friction. Macromolecules 45:2773–2782